ISSN 1063-7788, Physics of Atomic Nuclei, 2007, Vol. 70, No. 8, pp. 1386–1391. © Pleiades Publishing, Ltd., 2007.

NUCLEI
Theory

Octupole Excitations at High Spins in $A \sim 160$ Nuclei*

J. Kvasil[1)**], R. G. Nazmitdinov[2),3)], A. S. Sitdikov[4)], and P. Veselý[5)***]

Received October 31, 2006

Abstract—The yrast and yrare states of ^{162}Yb are studied within the cranked Nilsson model and random phase approximation. Special attention is paid to the analysis of experimental crossing points between different bands that form the yrast band. We found that, at the rotational frequency $\hbar\Omega > 0.3$ MeV, there is onset of strong octupole correlations. The results of calculations demonstrate good agreement with available experimental data.

PACS numbers: 21.10.Re, 21.60.Jz, 27.70.+q
DOI: 10.1134/S106377880708011X

1. INTRODUCTION

Octupole correlations are among important constituents of nuclear dynamics at low energy. Experimentally, they are manifested via enhanced dipole and octupole transitions, rotational bands of alternating parity, and low-lying octupole vibrational states (see for a review [1]). According to a general notion, octupole correlations are expected to be strong when pairs of orbitals from the intruder subshell (l, j) and the normal parity subshell $(l-3, j-3)$ are near the Fermi energy. Numerous calculations exploiting the intrinsic reflection symmetry breaking of a mean field—the macroscopic–microscopic approach combining the liquid-drop model with the Strutinsky shell correction method (cf. [2, 3]) and the microscopic HFB (HF) approach with effective nucleon–nucleon interaction (cf. [4, 5])—predict the existence of stable axial octupole deformation in the ground state for Ra–Th ($Z \sim 88$, $N \sim 134$) and Ba–Sm ($Z \sim 58$, $N \sim 88$) nuclei, where strong octupole instability is due to the coupling of $j_{15/2}$–$g_{9/2}$, $i_{13/3}$–$f_{7/2}$, $h_{11/2}$–$d_{5/2}$ orbitals.

It is a rare phenomenon, however, when shell effects may produce stable axial or nonaxial octupole deformed shapes in ground states for nuclei. In realistic calculations (cf. [1]), the potential energy surface is quite shallow, although such shapes are most likely in other mesoscopic systems (see, e.g., the discussion in [6]). Indeed, nuclear spectra show quite pronounced parity splitting at low angular momenta. Relatively weak dipole and octupole transitions observed at small rotational frequencies rather suggest that the nuclear potential is governed mainly by quadrupole deformations. However, with the increase in the rotational frequency, one observes a smooth decrease in the parity splitting in fairly few nuclei. These features are nicely reproduced within the cranking + HFB approaches with different effective nucleon–nucleon interaction that allow a reflection symmetry breaking. For example, good agreement was obtained between calculated and experimental data on the energy splitting of different parity states at nonzero angular momenta as well as for $B(E1)$ transition probabilities in $N = 88$ isotopes with the Gogny forces [7]. Dipole transitions in actinides are well described in [8] with aid of the cranked Skyrme Hamiltonian [9]. In the latter calculations, the onset of nonaxial octupole deformation at high spins was also found. The onset of nonaxial octupole deformations with the increase in the rotational frequency was already predicted for light nuclei within the cranking + HFB approach with the Skyrme [10] and the Gogny [11] interactions.

Theoretical and experimental studies of collective vibrations provide a direct way to shed light onto nuclear dynamics. A simple physical idea that the instability of a nuclear potential with respect to a given deformation implies a softening of the corresponding vibrational mode can be used as a guided-line in such studies. For example, a softening of the quadrupole vibrational mode can lead to the transition from axial

*The text was submitted by the authors in English.

[1)]Institute of Particle and Nuclear Physics, Charles University, Praha, Czech Republic.
[2)]Departament de Física, Universitat de les Illes Balears, Palma de Mallorca, Spain.
[3)]Bogolyubov Laboratory of Theoretical Physics, Joint Institute for Nuclear Research, Dubna, Russia.
[4)]Kazan State Power Engineering University, Kazan, Russia.
[5)]Physics Department, Charles University, Praha, Czech Republic.
**E-mail: kvasil@ipnp.troja.mff.cuni.cz
***E-mail: vesely@ipnp.troja.mff.cuni.cz

to nonaxial shapes (cf. [12]). For this purpose the cranked shell model that incorporates the random phase approximation (RPA) provides a powerful tool to illuminate the evolution of various correlations that evolve through dynamical shape fluctuations (vibrations) to the instability of a nuclear shape (see for octupole correlations in a simple model [13, 14]).

Recently, we developed a practical method based on the self-consistent solution of the cranked Nilsson model + monopole pairing (SCNM) for the yrast line and separable residual interactions, treated in the RPA, for the analysis of the low-lying excitations near the yrast line [15]. In contrast to previous studies of low-lying excitations at high spins, we paid special attention to the self-consistency between the mean field results and a description of low-lying excitations in the RPA. All the details of this approach are thoroughly discussed in [15] (2006). The analysis of M1 excitations [16], shape-phase transitions, and the behavior of the positive signature excitations at the backbending [15] confirmed the validity and vitality of this approach.

In this report, we discuss some results of the microscopic analysis of yrast and yrare rotational bands in ^{162}Yb, within the SCNM + RPA approach. In particular, we predict a drastic increase in dipole and octupole transitions from the negative parity states to the yrast states at $\hbar\Omega > 0.3$ MeV.

2. OUTLINE OF THE APPROACH

Our consideration is based on the Hamiltonian

$$\hat{H}_\Omega = \hat{H}_0 - \lambda_\tau \hat{N}_\tau - \Omega \hat{J}_x + V. \qquad (1)$$

The term $\hat{H}_0 = \hat{H}_{\rm N} + \hat{H}_{\rm add}$ contains the Nilsson Hamiltonian $\hat{H}_{\rm N}$ and an additional term that restores the local Galilean invariance of the Nilsson potential, broken in the rotating frame. The Nilsson potential naturally incorporates the deformation parameters of a nuclear shape [17]. The chemical potentials λ_τ ($\tau = n$ or p) are determined so as to give correct average particle numbers $\langle \hat{N}_\tau \rangle$. Hereafter, $\langle \ldots \rangle$ means the averaging over the mean field vacuum (yrast) state at a given rotational frequency Ω. The interaction V includes separable monopole pairing, monopole–monopole, quadrupole–quadrupole, and spin–spin terms to describe the positive parity states and dipole–dipole and octupole–octupole terms for the negative parity states. All multipole and spin-multipole operators have a good isospin T and signature $r = \pm 1$ (see the properties of the matrix elements in [18]). They are expressed in terms of doubly stretched coordinates $\tilde{x}_i = (\omega_i/\omega_0)x_i$, which ensure the self-consistent conditions at the equilibrium deformation. Some details about the model Hamiltonian (1) can be found in [15].

We solve the Hartree–Bogolyubov (HB) equations for the Hamiltonian (1) self-consistently at each rotational frequency. However, in the vicinity of the backbending, the solution of nonlinear HB equations becomes highly unstable. In order to avoid unwanted singularities for certain values of Ω, we followed the phenomenological prescription [19] for the definition of the pairing gap parameter (see details in [15]). Parameters of the Nilsson potential were taken from [20]. In our calculations, we include all shells up to $N = 9$. Near the transition point, we extended our configuration space up to $N = 10$ shells. The difference between results from the former and the latter cases was small and all presented results are obtained with $N = 0{-}9$ shells. In contrast to standard calculations with the Nilsson potential, based on a "single stretched" coordinate method (cf. [17]), we take into account the $\Delta N = 2$ mixing exactly, which improves the accuracy of the mean field calculations.

The consistency between the mean field and the residual interactions of the Hamiltonian (1) was achieved by varying the strength constants of the pairing and multipole interactions in the RPA. It results in the separation of collective excitations from those that are related to the symmetries broken by the mean field. In particular, we solve the RPA problem (see [15]) separately for the positive (negative) signature and both parities under conditions

$$\left[\hat{H}_\Omega(^{\pi=+}_{r=+}), \hat{N}_\tau\right] = 0, \quad \left[\hat{H}_\Omega(^{\pi=-}_{r=+}), \hat{P}_x\right] = 0, \quad (2)$$
$$\left[\hat{H}_\Omega(^{\pi=+}_{r=+}), \hat{J}_x\right] = 0, \quad \left[\hat{H}_\Omega(^{\pi=+}_{r=-}), \hat{\Gamma}^\dagger\right] = \Omega\hat{\Gamma}^\dagger,$$

where

$$\hat{\Gamma}^\dagger = \frac{\hat{J}_z + i\hat{J}_y}{\sqrt{2\langle \hat{J}_x \rangle}}, \quad \hat{\Gamma} = (\hat{\Gamma}^\dagger)^\dagger, \quad [\hat{\Gamma}, \hat{\Gamma}^\dagger] = 1. \qquad (3)$$

Two zero solutions are associated with the violation of the particle number (for protons and for neutrons). The other two are related to the translational and spherical symmetries of the mean field. The last equation yields a negative signature solution $\hbar\omega_\lambda = \hbar\Omega$, which describes a collective rotational mode arising from the symmetries broken by the external rotational field (the cranking term). Equations (2) and (3) ensure the separation of the "spurious" or redundant solution from the intrinsic excitations.

3. DISCUSSION OF RESULTS

To analyze experimental data [21] on low-lying excited states near the yrast line of ^{162}Yb, we construct the experimental Routhian function

$$R_\nu(\Omega) = E_\nu(\Omega) - \hbar\Omega_\nu I(\Omega), \qquad (4)$$

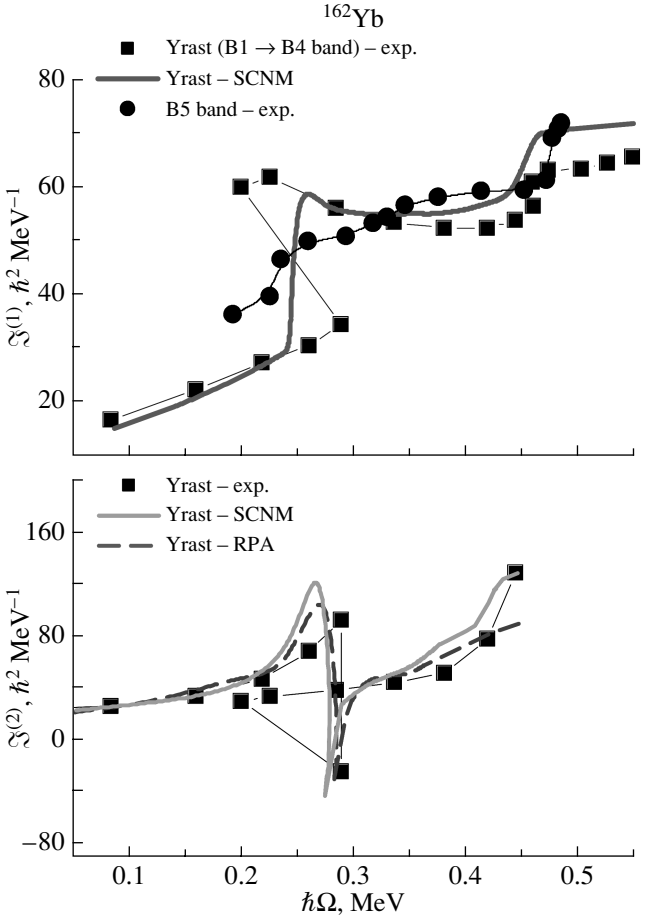

Fig. 1. The kinematic $\Im^{(1)}(\Omega) = \langle \hat{J}_x \rangle / \Omega$ (top) and dynamic $\Im^{(2)}(\Omega)$ (bottom) moments of inertia are compared with the corresponding experimental values (■). Experimental values are connected by a thin line to guide the eye. The experimental values for the kinematic moment of inertia for the lowest negative parity band are also shown in the top panel (●). The calculated values of the kinematic and dynamic moments of inertia for the yrast line are connected by solid curves. The dashed curve displays the behavior of the Thouless–Valatin moment of inertia calculated in the RPA (bottom).

$$\hbar\Omega_\nu(I) = \frac{E_\nu(I+1) - E_\nu(I-1)}{2}$$

from experimental levels $E_\nu(I)$ for each observed rotational band ν ($\nu = \text{yrast}, \beta, \gamma, \ldots$). By means of this procedure, we define the experimental excitation energy in the rotating frame $\hbar\omega_\nu(\text{exp.}) = R_\nu(\Omega) - R_{\text{yr}}(\Omega)$ as a function of the rotational frequency Ω [22]. This energy can be directly compared with the RPA solutions, $\hbar\omega_\nu$, found at a given rotational frequency. Standard definitions are used to calculate the experimental kinematic $\Im^{(1)}_{\text{exp},\nu}(\Omega(I)) = \hbar^2 2I/(E_\nu(I+1) - E_\nu(I-1))$ and the dynamic $\Im^{(2)}_{\text{exp},\nu} = \hbar dI/d\Omega = 2\hbar/(\Omega_\nu(I+1) - \Omega_\nu(I-1))$ moments of inertia for each rotational band ν.

The experimental level sequences for all observed up-to-date rotational bands in ^{162}Yb are taken from [21], which is regularly updated. Six rotational bandsare observed, which we numerate as rotational bands B1, …, B6 in accordance with [21]. We recall that all rotational states are classified by the signature $r = \exp(-i\pi\alpha)$ leading to selection rules for the total angular momentum $I = \alpha + 2n$, $n = 0, \pm1, \pm2 \ldots$. In particular, in even–even nuclei, the yrast band characterized by the positive signature quantum number $r = +1 (\alpha = 0)$ consists of even spins only. The negative signature bands $r = -1\,(\alpha = 1)$ consist of odd spins only.

The bands B1 (ground band) and B2 (β band), levels with even angular momenta of the band B3 (γ band), and the band B4 are characterized by a positive parity and a positive signature ($\pi = +, \alpha = 0$). There is only one level ($I = 3$, γ band (B3)) that belongs to the sector of the positive parity and the negative signature. The band B5 is of negative parity and negative signature, while the band B6 belongs to the sector ($\pi = -, \alpha = 0$). The band B4 crosses the band B1 at the rotational frequency $\hbar\Omega \approx 0.265$ MeV

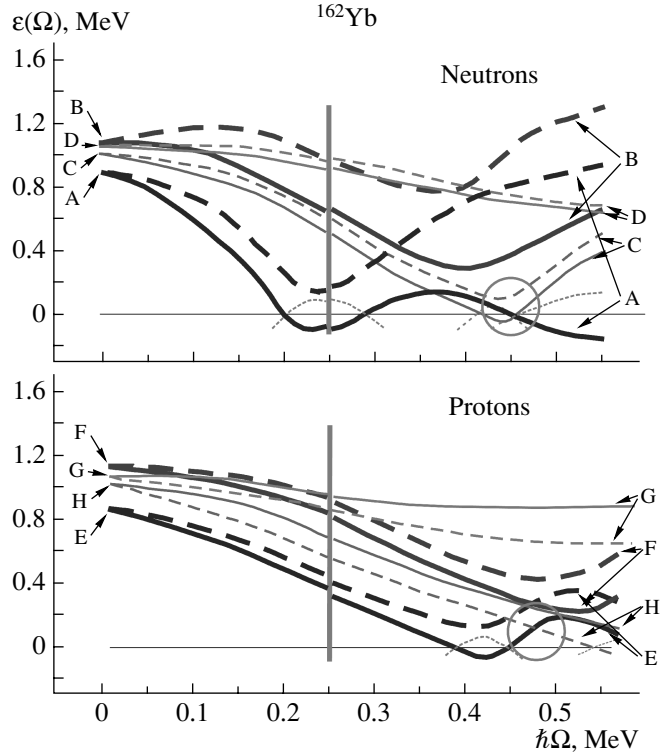

Fig. 2. Lowest quasineutron (top) and quasiproton (bottom) energies for ^{162}Yb as a function of the rotational frequency Ω. Thick (thin) lines are used for the positive (negative) parity states. The positive (negative) signature states are connected by solid (dashed) curves. At $\Omega = 0$, levels A, B, C, and D in the upper panel correspond to the neutron Nilsson states 3/2[651] (subshell $i_{13/2}$), 1/2[660] (subshell $i_{13/2}$), 3/2[521] (subshell $h_{9/2}$), and 5/2[521] (subshell $f_{7/2}$), respectively; and levels E, F, G, and H in the lower panel correspond to the proton Nilsson states 7/2[523] (subshell $h_{11/2}$), 9/2[514] (subshell $h_{11/2}$), 5/2[402] (subshell $d_{5/2}$), and 7/2[404] (subshell $g_{7/2}$), respectively. The shape transition point $\gamma = 0 \to \gamma \neq 0$ is denoted by the vertical line. Regions where the positive parity and negative parity quasiparticle orbits cross each other near the zero energy are surrounded by circles. In these regions, strong octupole correlations are expected in the rotational states near the yrast line.

and becomes the yrast one for $\hbar\Omega > 0.265$ MeV. The change of the yrast line structure at $\hbar\Omega \approx 0.265$ MeV is associated with the backbending (see experimental points in Fig. 1 for the kinematic and dynamic moments of inertia). Almost a zero energy gap between the both negative parity bands (B5 and B6) and the yrast line, observed at $\hbar\Omega \geq 0.45$ MeV, implies the presence of strong octupole correlations (see below).

One of the strongest tests of the self-consistency microscopic calculations is the comparison of the dynamical moment of inertia $\mathfrak{J}^{(2)}_{HB} = -d^2E_{HB}/d\Omega^2 = d\langle\hat{J}_x\rangle/d\Omega$ ($E_{HB} = \langle\hat{H}_\Omega\rangle$) and the Thouless–Valatin $\mathfrak{J}_{\rm TV}$ moments of inertia calculated in the RPA. They must coincide (see the results for exactly solvable model in [23]) if one found a *self-consistent mean field minimum and spurious solutions are separated from the physical ones*. The mode associated with the rotation about the x axis allows one to determine the Thouless–Valatin moment of inertia $\mathfrak{J}_{\rm TV}$ using the positive signature term of the full Hamiltonian

$$[\hat{H}_\Omega(^{\pi=+}_{r=+}), i\hat{\Phi}] = \frac{\hat{J}_x}{\mathfrak{J}_{\rm TV}}, \quad [\hat{\Phi}, \hat{J}_x] = i. \qquad (5)$$

Here, the angle operator $\hat{\Phi}$ is the canonical partner of the angular momentum operator $\hat{J}_x$.

Figure 1 demonstrates a good self-consistency between the mean field and RPA calculations, indeed. The triaxiality of the mean field sets at the rotational frequency $\hbar\Omega_c \approx 0.250$ MeV, which triggers the backbending observed in ^{162}Yb. The transition point obtained in the HB calculations is in good agreement with the experimental value $\hbar\Omega_c \approx 0.265$ MeV. We emphasize that the inclusion of the additional term in the Hamiltonian (1) is crucial to achieve a good description of the experimental inertial properties.

To understand the quasiparticle structure near the transition point, we trace the rotational evolution of quasiparticle orbitals in the rotating frame (routhians) as a function of the equilibrium parameters (ε,

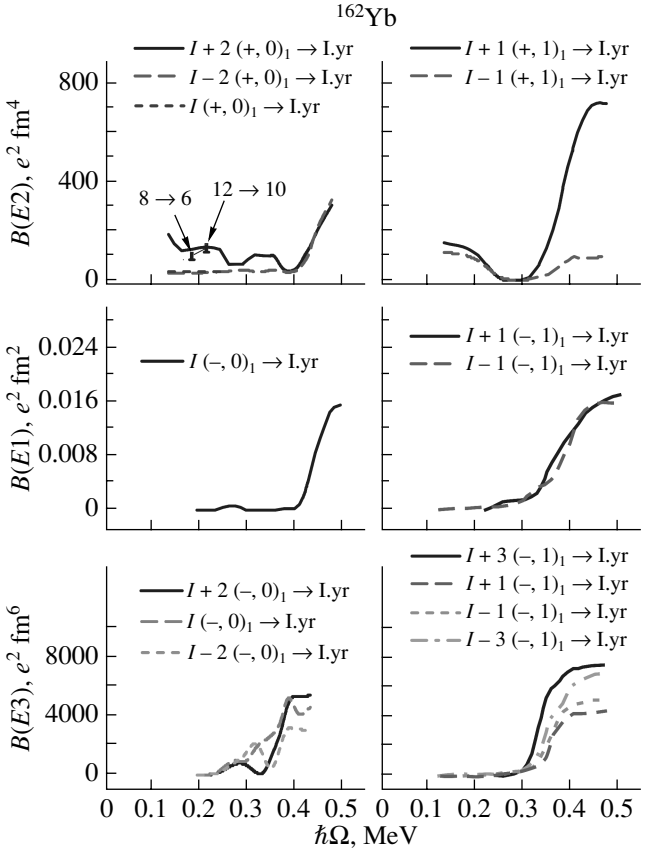

Fig. 3. Reduced $B(E2)$, $B(E1)$, and $B(E3)$ transition probabilities from the lowest one-phonon bands to the yrast line in ^{162}Yb. Each excited state with the angular momentum I is characterized by two quantum numbers: the parity $\pi = \pm$ and the signature $\alpha = 0, 1$ (or $r = +1, -1$, respectively). Left (right) panels correspond to the transition with $\Delta I =$ even ($\Delta I =$ odd) from the lowest positive (negative) signature states, i.e., from the states with $\alpha = 0(1)$. The quadrupole transitions are considered from the positive parity phonon states, while the dipole and octupole transitions are from the negative parity phonon states. The arrows indicate experimental values.

γ, Δ). At $\Omega = 0$, each orbital is characterized by the asymptotic Nilsson quantum numbers. However, these numbers lose their validity in the rotating case owing to a strong mixing. Hereafter, they are used only for convenience. The analysis of the routhians for neutrons (Fig. 2, top) and for protons (Fig. 2, bottom) indicates that the lowest quasicrossings occur at $\hbar\Omega \approx 0.245(0.41)$ MeV for the neutron (proton) system in ^{162}Yb. We recall that the shape-phase transition takes place at $\hbar\Omega_c \approx 0.265$ MeV. The proximity of the critical point to the two-quasiparticle neutron quasicrossing in ^{162}Yb suggests that the alignment of a pair $i_{13/2}$ is the main mechanism that drives the nucleus to triaxial shapes (cf. [24]). From Fig. 2, one observes that, in the region $\hbar\Omega \approx 0.45{-}0.5$ MeV, the positive parity quasiparticle orbits cross the negative parity ones near the Fermi energy. In particular, the neutron positive parity orbit (A) originating from the $i_{13/2}$ subshell crosses the negative parity orbit (C) from the $h_{9/2}$ subshell near zero energy at $\hbar\Omega =$ 0.45 MeV. A similar pattern is observed for protons: a crossing of the $h_{11/2}$ orbit (E) with $g_{7/2}$ orbit (H) is found at $\hbar\Omega \approx 0.48$ MeV.

As was mentioned above, the zero energy gap between the lowest negative parity and negative signature rotational bands and the yrast line at large Ω indicates a possible presence of the nonzero octupole deformation in the corresponding yrast line states. This idea is supported by our RPA + SCNM calculations. The collectivity of the lowest positive and negative parity RPA solutions of both signatures increases remarkably with the increase in the rotational frequency. The results for the reduced transition probabilities $B(E1)$ and $B(E3)$ from the lowest phonon states to yrast line states at $\hbar\Omega >$ > 0.3 MeV evidently demonstrate the onset of strong octupole correlations (see Fig. 3). The collectivity of the lowest negative parity one-phonon states with energies going to zero at $\hbar\Omega > 0.3$ MeV emerges from several two-quasiparticle components with the largest neutron $i_{13/2}{-}h_{9/2}$ (AC in Fig. 2) and proton

$h_{11/2}-g_{7/2}$ (EH in Fig. 2) ones. We speculate that the growing collectivity of low-energy negative parity states with the increase in the rotational frequency signal on a possible shape transition from plain quadrupole deformed shapes to quadrupole–octupole ones occurs at $\hbar\Omega > 0.4$ MeV. We also found that the B(E2) transitions from the positive parity states increase with the rotational frequency as well. It may be related to the wobbling excitations which are a subject of separate studies.

Summarizing, we found that a shape transition from the axially symmetric to the nonaxial shapes occurs at $\hbar\Omega \approx 0.25$ MeV. The internal structure of the one-phonon ($\pi = +, \alpha = 0$) band, which crosses the ground band, has almost a pure two-quasiparticle character originating from the $i_{13/2}$ neutron shell. The transition point is in good agreement with the experimental value $\hbar\Omega_c \approx 0.265$ MeV at which the backbending occurs in the lab frame. We found at $\hbar\Omega \approx 0.4$ MeV (in an agreement with the experimental data) the onset of the degeneracy between the lowest negative parity bands of both signatures and the yrast line. The corresponding negative parity phonon states forming these bands are strongly collective. We predict strong $B(E1)$ and $B(E3)$ transitions from these negative parity bands to the yrast line (see Fig. 3) at $\hbar\Omega > 0.3$ MeV.

4. ACKNOWLEDGMENTS

This work is a part of the research plan MSM 0021620834 supported by the Ministry of Education of the Czech Republic. It was partially supported by the Ministry of Education and Science of Spain (MEC), grant FIS2005-02796. R.G.N. gratefully acknowledges the support from the Ramón y Cajal programme (Spain).

REFERENCES

1. P. A. Butler and W. Nazarewicz, Rev. Mod. Phys. **68**, 349 (1996).
2. P. Möller and S. G. Nilsson, Phys. Lett. B **31**, 283 (1970).
3. W. Nazarewicz et al., Nucl. Phys. A **429**, 269 (1984).
4. P. Bonche et al., Phys. Lett. B **175**, 387 (1986).
5. J. L. Egido and L. M. Robledo, Nucl. Phys. A **518**, 475 (1990).
6. W. D. Heiss, R. A. Lynch, and R. G. Nazmitdinov, Phys. Rev. C **60**, 034303 (1999).
7. F. Garrote, J. L. Egido, and L. M. Robledo, Phys. Rev. Lett **80**, 4398 (1998).
8. A. Tsvetkov, J. Kvasil, and R. G. Nazmitdinov, J. Phys. G **28**, 2187 (2002).
9. J. Dobaczewski and J. Dudek, Comput. Phys. Commun. **131**, 164 (2000).
10. M. Yamagami and K. Matsuyanagi, Nucl. Phys. A **672**, 123 (2000).
11. T. Tanaka, R. G. Nazmitdinov, and K. Iwasawa, Phys. Rev. C **63**, 034309 (2001).
12. W. D. Heiss and R. G. Nazmitdinov, Pis'ma Zh. Eksp. Teor. Fiz. **72**, 157 (2000) [JETP Lett. **72**, 106 (2000)]; Phys. Rev. C **65**, 054304 (2002).
13. R. Nazmitdinov and S. @Aberg, Phys. Lett. B **289**, 238 (1992); T. Nakatsukasa, and K. Matsuyanagi, and S. Mizutori, Prog. Theor. Phys. **87**, 607 (1992).
14. T. Nakatsukasa et al., Phys. Rev. C **53**, 2213 (1996).
15. J. Kvasil and R. G. Nazmitdinov, Phys. Rev. C **69**, 031304(R) (2004); Pis'ma Zh. Eksp. Teor. Fiz. **83**, 227 (2006) [JETP Lett. **83**, 187 (2006)]; Phys. Rev. C **73**, 014312 (2006).
16. J. Kvasil, N. Lo Iudice, R. G. Nazmitdinov, et al., Phys. Rev. C **69**, 064308 (2004).
17. S. G. Nilsson and I. Ragnarsson, *Shapes and Shells in Nuclear Structure* (Cambridge Univ. Press, Cambridge, 1995).
18. J. Kvasil et al., Phys. Rev. C **58**, 209 (1998).
19. R. Wyss et al., Nucl. Phys. A **511**, 324 (1990).
20. A. K. Jain et al., Rev. Mod. Phys. **62**, 393 (1990).
21. http://www.nndc.bnl.gov/nudat2/.
22. R. G. Nazmitdinov, Yad. Fiz. **46**, 732 (1987) [Sov. J. Nucl. Phys. **46**, 412 (1987)].
23. R. G. Nazmitdinov, D. Almehed, and F. Dönau, Phys. Rev. C **65**, 041307(R) (2002).
24. S. Frauendorf and F. R. May, Phys. Lett. B **125**, 245 (1983).